

# Atomistic origin of rapid crystallization of Ag-doped Ge–Sb–Te alloys: A joint experimental and theoretical study

B. Prasai, M. E. Kordesch, D. A. Drabold\*, and G. Chen\*\*

Department of Physics and Astronomy, Ohio University, Athens, OH 45701, USA

Received 28 February 2013, revised 25 April 2013, accepted 6 May 2013

Published online 3 June 2013

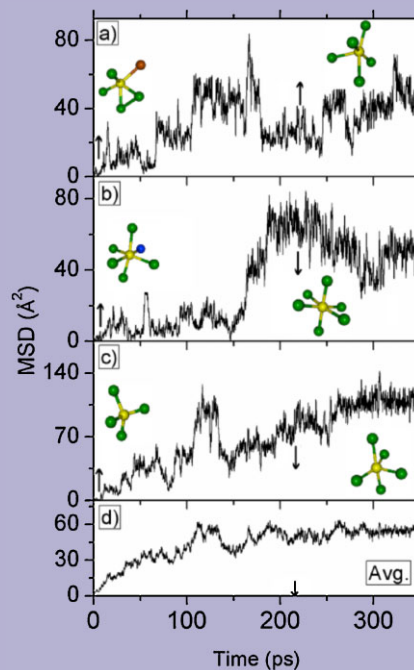
**Keywords** *ab initio* simulation, chalcogenide glass, phase-change memory materials, phase transitions

\* Corresponding author: e-mail drabold@ohio.edu, Phone: 740-593-1715, Fax: 740-593-0433

\*\* e-mail cheng3@ohio.edu

We have applied extended X-ray absorption fine structure (EXAFS) analyses and *ab initio* molecular dynamics (AIMD) simulations to study the structure of Ag-doped (up to 42%)  $\text{Ge}_1\text{Sb}_2\text{Te}_4$  alloys. The computer models are consistent with EXAFS experiments, and reveal that the Ge environment is significantly modified by Ag doping, whereas those of Sb and Te are barely affected (except for high Ag concentrations), and suggest that Ag prefers bonding with Te. Doping with Ag promotes the conversion of Ge from tetrahedral to octahedral, and enhances the speed of crystallization of Ge–Sb–Te (GST) alloys as predicted by MD simulation. Our study sheds light on the atomistic mechanism of rapid crystallization of GST alloys, and enhancement by Ag doping.

Mean-square displacements (MSDs), depicting the hopping of individual silver atoms in the silver-doped GeSbTe phase-change memory material (PCMM).



© 2013 WILEY-VCH Verlag GmbH & Co. KGaA, Weinheim

**1 Introduction** Chalcogenide alloy systems have proven to be among the most flexible and useful materials. They are the basis of rewritable DVD technology [1], phase change and conducting bridge computer memory [2, 3], they exhibit exotic and apparently unique photo-response, including the opto-mechanical effect [4]. Chalcogenide glasses doped with transition metals are solid electrolytes with many potential applications [3].

GST alloys near the pseudobinary  $\text{GeTe-Sb}_2\text{Te}_3$  tie line are widely accepted phase-change memory materials (PCMM) for application in optical and electronic memories because of their outstanding switching performance [5], and efforts have been devoted to improve material properties such as switching speed, phase transition temperature, and thermal stability. One way to modify the physical properties of PCMM is by doping or alloying with other elements.

Doping has been studied in the past few years, either by experimental methods or theoretical/computational methods [6–15].

Experimental investigations suggest that for  $\text{Ge}_2\text{Sb}_2\text{Te}_5$ , the crystallization temperature is elevated by C, N, Mo, and Zn doping, whereas Sn and Bi lower the crystallization temperature [6–8, 10, 11]. Doping also affects the speed of crystallization. It has been reported that Ag in  $\text{Ge}_2\text{Sb}_2\text{Te}_5$  accelerates the crystallization [9].

*Ab initio* molecular dynamics (AIMD) investigations suggest that dopants like C and N affect the local order of amorphous  $\text{Ge}_2\text{Sb}_2\text{Te}_5$  by elevating the fraction of tetrahedral Ge atoms and hence enhancing the thermal stability [12–14]. It has also been reported that Si and O dopants slow the crystallization of  $\text{Ge}_2\text{Sb}_2\text{Te}_5$  whereas Ag dopants enhance the crystallization speed of  $\text{Ge}_2\text{Sb}_2\text{Te}_5$  [13, 15].

The traditional trial and error approach to materials discovery has been a major obstacle to identifying new PCMM with improved properties because of our incomplete understanding of the structure–property relations. As properties of PCMM accrue from the structure, knowledge of the structure and dynamics of these materials is essential. A deep understanding of the PCMM requires a comprehensive approach that involves coupled theory and experiment. In this paper, we present a joint experimental/theoretical study of silver doped phase change GST alloy. Building on a preliminary report on the  $\text{Ge}_2\text{Sb}_2\text{Te}_5$  [15], we detail the role of Ag in the network, and its impact on crystallization in a different stoichiometry. We address two questions: (1) How does Ag affect the structure of GST alloys? (2) How does Ag affect the speed of crystallization of GST? To answer these questions, we perform an extended X-ray absorption fine structure (EXAFS) analysis and density functional (DF) simulations to study the local structure of Ag doped amorphous  $\text{Ge}_1\text{Sb}_2\text{Te}_4$ . DF simulations of such materials are particularly helpful, as they provide structural information that is not readily obtained from EXAFS. Direct comparisons of EXAFS measurements and simulations demonstrate how Ag converts tetrahedral Ge into octahedral, and provides new directions in the exploration for improved materials. Hegedus and Elliott were the first to show that direct *ab initio* simulation of crystallization is possible [16], a very remarkable result. We exploit this discovery in our work.

## 2 Methods

### 2.1 Experimental

**2.1.1 Sample preparation**  $(\text{Ge}_1\text{Sb}_2\text{Te}_4)_{(100-x)/7}\text{Ag}_x$  ( $x = 0, 7, 14, 20$ , and  $40$ ) thin films were prepared by radio frequency sputtering (13.56 MHz) from a  $\text{Ge}_1\text{Sb}_2\text{Te}_4$  target (50 mm in diameter) in argon at an average power of 5 Watts  $\text{cm}^{-2}$ . Silver plates measuring 8 mm  $\times$  15 mm  $\times$  1 mm were placed on the target, with thin Tantalum foil placed between the plates and the  $\text{Ge}_1\text{Sb}_2\text{Te}_4$  target. Typical Ar pressure was 8 mTorr. Thickness of the films was measured with a quartz crystal thickness monitor.  $\text{Ge}_1\text{Sb}_2\text{Te}_4$ -Ag films with five different Ag dopant levels (0–40.2%) were fabricated. The compositions of the

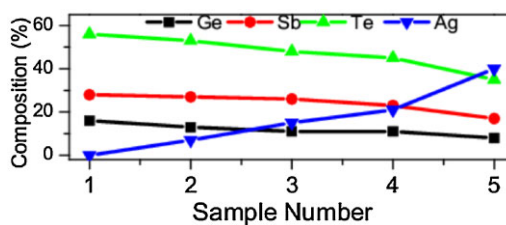


**Figure 1** Sample compositions (in %) in Ge-Sb-Te-Ag films as measured by EDXS. The uncertainties lie within 2%.

$\text{Ge}_1\text{Sb}_2\text{Te}_4$ -Ag films were obtained by energy dispersive X-ray spectroscopy (EDXS). Figure 1 presents the compositions of the  $\text{Ge}_1\text{Sb}_2\text{Te}_4$ -Ag films used in the present study.

**2.1.2 Experiment and analysis** The EXAFS experiment was conducted at the 5-BM beamline of the Advanced Photon Source (APS) at Argonne National Laboratory. The Ge K-edge (11.104 keV) EXAFS spectrum was measured at room temperature under transmission mode with ionization chambers, and Sb (30.491 KeV) and Ag (25.514 KeV) K-edge spectra were measured under fluorescence mode with a 13-element Ge detector. A reference sample that contains the three elements was used to calibrate the X-ray energy for different scans at the same K edges. The EXAFS data was analyzed with the FEFF [17] code (for phase shift information) using a model of  $(\text{Ge}_1\text{Sb}_2\text{Te}_4)_{(100-x)/7}\text{Ag}_x$  and the structural parameters were optimized by using ARTEMIS [18].

## 2.2 Modeling

**2.2.1 Molecular dynamics simulations** AIMD simulations were performed using the Vienna *Ab initio* Simulation Package (VASP) code to generate models of amorphous  $(\text{Ge}_1\text{Sb}_2\text{Te}_4)_{(100-x)/7}\text{Ag}_x$  [19]. We prepared four computer models of Ag-doped  $\text{Ge}_1\text{Sb}_2\text{Te}_4$  materials with Ag concentration ( $x$ ) ranging 0–42%:  $x = 0$  (15 Ge atoms, 30 Sb atoms, and 60 Te atoms),  $x = 6$  (15 Ge atoms, 30 Sb atoms, 60 Te atoms, and 7 Ag atoms),  $x = 12$  (15 Ge atoms, 30 Sb atoms, 60 Te atoms, and 14 Ag atoms), and  $x = 42\%$  (10 Ge atoms, 20 Sb atoms, 40 Te atoms, and 50 Ag atoms). The models were prepared by following the methods of Ref. [15]. Each model was equilibrated at 300 K for at least 10 ps, and EXAFS data was simulated by using the FEFF code [17] from the configurations predicted at every 0.25 ps, and subsequently, statistically averaged. At least two independent models were generated to investigate the model dependence of the structural properties. The structures (up to 10% Ag concentrations) were annealed at 650 K until crystallization occurred.

**3 Results and discussion** Figure 2 shows  $k^3$  weighted Ge, Sb, and Ag Fourier transformed EXAFS spectra ( $\chi(r)$ ) of Ag doped  $\text{Ge}_1\text{Sb}_2\text{Te}_4$  samples (uncorrected for phase shifts) with different Ag concentration ( $x$ ). Beside

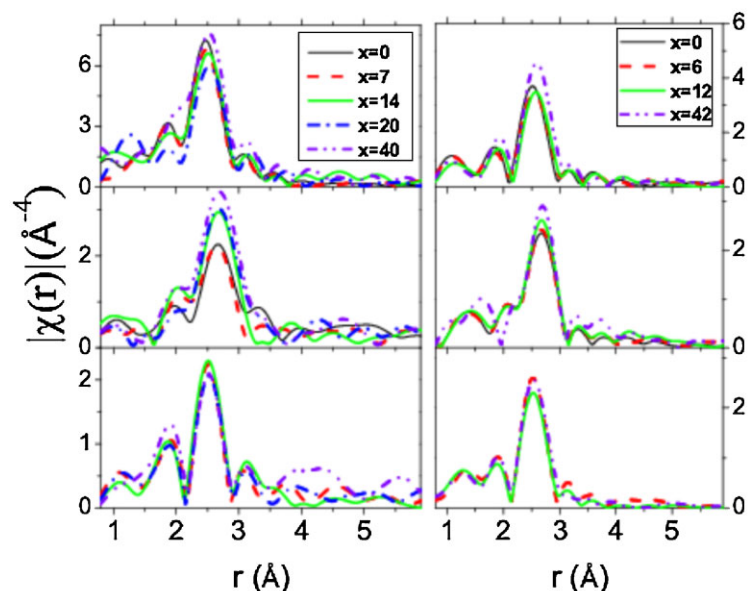


**Figure 2** Magnitude of  $k^3$  weighted  $\chi(r)$  spectra (uncorrected for phase shift) as a function of Ag concentration.  $k$  ranges chosen for the Fourier transform are: 3–10  $\text{\AA}^{-1}$  for Ge K-edge spectra (top left), 4–10  $\text{\AA}^{-1}$  for Sb K-edge spectra (middle left) and 2–10  $\text{\AA}^{-1}$  for Ag K-edge spectra (bottom left). Figures on the right are the  $\chi(r)$  spectra obtained from the FEFF simulations at 300 K.

the main peaks, we observed smaller peaks near 1.0–2.0  $\text{\AA}$  mainly in Ge and Sb edge spectra. These peaks are mostly due to a termination effect caused by finite  $k$  range of Fourier transform and thus are neglected in the analysis. To obtain the structural parameters, these  $\chi(r)$  spectra were fitted with ARTEMIS using the appropriate scattering paths calculated from a  $(\text{Ge}_1\text{Sb}_2\text{Te}_4)_{(100-x)/7}\text{Ag}_x$  model via FEFF [17, 18]. Since the atomic numbers and radii of Sb and Te are close to each other, and they may not readily be distinguishable via EXAFS, the contribution from Sb neighbor atoms was replaced by Te atoms. This is appropriate in the analysis because the coordination number analysis in the AIMD generated models confirms that the probability of finding Sb as neighbor is less than 0.15 for all Ge, Te, Sb, and Ag central atoms. The fitted average bond lengths and the coordination numbers are illustrated in Figs. 3 and 4, respectively.

As a benchmark, we start with Sample 1, whose composition (Ge = 16, Sb = 28, and Te = 56) is close to composition of  $\text{Ge}_1\text{Sb}_2\text{Te}_4$  within the experimental uncertainty (2%). The average Ge–Te bond length of 2.61  $\text{\AA}$  and Sb–Te bond length of 2.84  $\text{\AA}$  obtained from our EXAFS analysis are consistent with those reported in a previous study for a- $\text{Ge}_1\text{Sb}_2\text{Te}_4$ , and are similar to those previously reported for amorphous  $\text{Ge}_2\text{Sb}_2\text{Te}_5$  that also lie on the same pseudo-binary line of Ge–Te and  $\text{Sb}_2\text{Te}_3$  [20–22]. The structural similarities between slightly off-stoichiometric GST alloys and stoichiometric GST alloys have been confirmed by Caravati et al. [23]. However both the Ge–Te and Sb–Te bond lengths are shorter than those obtained from DF calculations [16, 23–25]. The Ge and Sb coordination numbers of 3.0(0.4) and 2.9(0.6) obtained from our EXAFS analysis are similar to the ones for amorphous  $\text{Ge}_1\text{Sb}_2\text{Te}_4$  as reported previously in Ref. [20] (*i.e.*, 3.3(0.3) for Ge and 2.9(0.4) for Sb). These numbers are consistent with those obtained from DF calculations of a- $\text{Ge}_1\text{Sb}_2\text{Te}_4$  (3.7 for Ge

and 3.6 for Sb) presented herein and those reported previously (3.5 for Ge and 3.8 for Sb) by Raty et al. [26].

In Ag-doped a- $\text{Ge}_1\text{Sb}_2\text{Te}_4$  the average Ge–Te bond length increases with Ag concentration while other bonds (mainly Sb–Te and Ag–Te) remain unchanged. These experimental results are consistent with both the EXAFS simulations based on the models as well as the direct partial pair correlation functions (PPCF) analysis (Fig. 3). The change in Ge–Te bond length can be linked to the change in the fraction of Ge in tetrahedral environment with shorter Ge–Te bond distribution. Ge has two environments (defective octahedral with longer Ge–Te average bond length and tetrahedral with shorter Ge–Te average bond

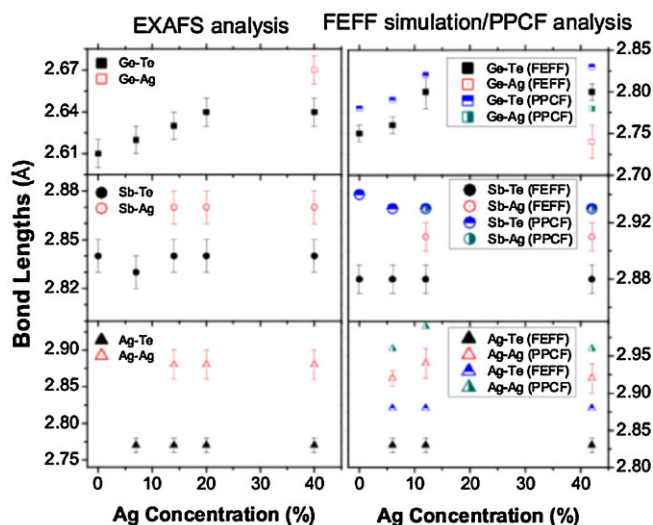


**Figure 3** Comparison of bond lengths obtained from EXAFS analysis (left) and FEFF/MD simulations (right).

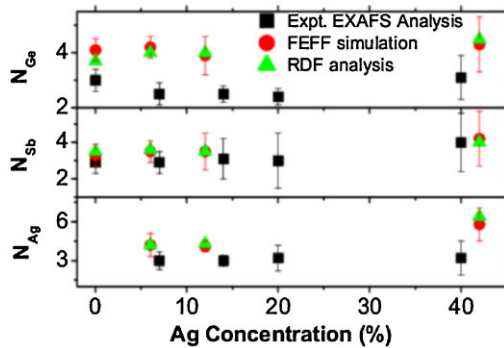


**Figure 4** Coordination numbers in  $a\text{-(Ge}_1\text{Sb}_2\text{Te}_4)_{(100-x)/7}\text{Ag}_x$  samples and models.

length), as depicted in the Ge-centered bond angle distribution (see Fig. 5 and Ref. [27]). When  $\text{Ge}_1\text{Sb}_2\text{Te}_4$  is doped with Ag, the Ge environment is significantly modified, so that the fraction of tetrahedrally bonded Ge is reduced as compared to the octahedral (distorted) Ge. The modification to the Ge–Te bonding configuration is reflected in the Ge-centered angle distribution (Fig. 5) where the suppression of the peak near  $110^\circ$  can be observed. Furthermore, the significant variation in the bond angle distribution explains the rearrangement of Ge atoms that could otherwise occupy tetrahedral sites. The modification of the tetrahedral geometry can also be explained through the local order parameter [27, 28]  $q$  given by

$$q = 1 - \frac{3}{8} \sum_i \sum_{k>i} \left( \frac{1}{3} + \cos\theta_{ijk} \right)^2,$$

in which the sum runs over the nearest neighbors of the central atom  $j$ . Figure 6 presents the distribution of  $q$  for Ge atoms.  $q = 1$  represents the ideal tetrahedral geometry whereas  $q = 0$  represents the perfect octahedral site. It is also clear from the figure that the fraction of tetrahedral Ge is reduced in consistent with the bond angle distributions. The increase in the fraction of Ge atoms in the distorted

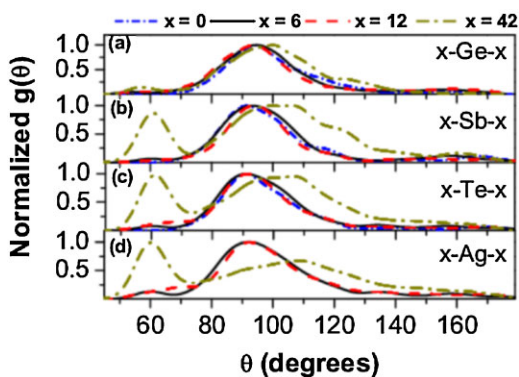


**Figure 5** Normalized bond angle distributions in  $a\text{-(Ge}_1\text{Sb}_2\text{Te}_4)_{(100-x)/7}\text{Ag}_x$ .

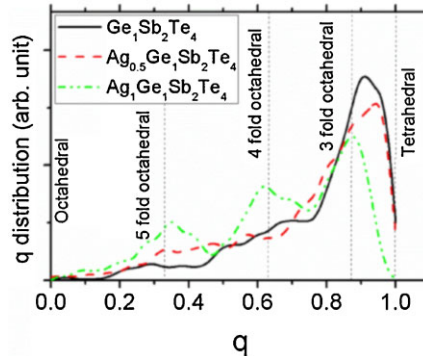


**Figure 6** Distribution of the local order parameter  $q$  for Ge in  $\text{Ge}_1\text{Sb}_2\text{Te}_4$ ,  $\text{Ag}_{0.5}\text{Ge}_1\text{Sb}_2\text{Te}_4$ , and  $\text{Ag}_1\text{Ge}_1\text{Sb}_2\text{Te}_4$ . A cut-off distance of 3.2 Å was chosen.

octahedral sites relative to that in tetrahedral sites explains the increase in average Ge–Te bond length. This increase could yield the faster crystallization when the GST alloy is doped with Ag, as the octahedral Ge is believed to be one of the members of square rings which are known as “seeds” of crystallization [16]. Faster crystallization induced by Ag doping of GST was reported experimentally by Song et al. [9].

The speed of crystallization of Ag doped  $a\text{-Ge}_1\text{Sb}_2\text{Te}_4$  was analyzed from AIMD simulations. Figure 7 shows the time evolution of the total energy of Ag doped and undoped  $\text{Ge}_1\text{Sb}_2\text{Te}_4$  (up to 12%) at 650 K. An abrupt reduction in the total energy is observed, associated with the amorphous-crystalline transition. The time associated with the transition is inversely proportional to the speed of the transition. The estimated crystallization time in the three models with Ag concentrations of 0, 6, and 12% are 330, 220, and 160 ps, respectively. It is clear that Ag doping increases the speed of the phase transition. The faster crystallization of Ag-doped  $\text{Ge}_2\text{Sb}_2\text{Te}_5$  is also reported by Prasai et al. from AIMD simulations [15].

We computed mean-squared displacements (MSDs) for Ag atoms throughout the crystallization process of

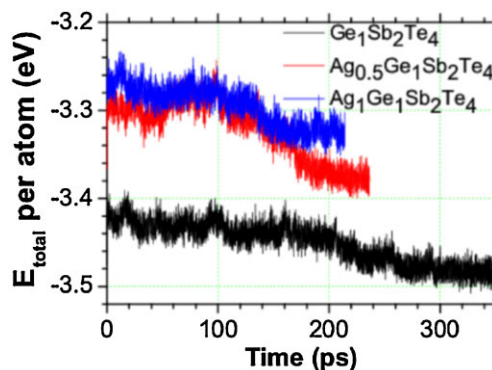


**Figure 7** Time evolution of the total energy of Ag doped  $\text{Ge}_1\text{Sb}_2\text{Te}_4$  at 650 K, showing a transition from the amorphous to crystalline state.

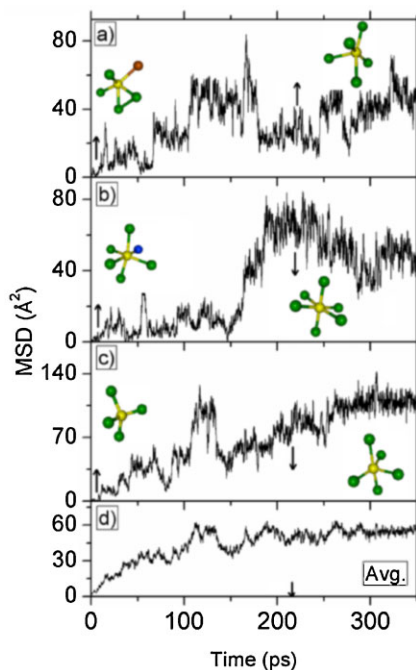


**Figure 8** Dynamics of Ag atoms in  $\text{Ag}_{0.5}\text{Ge}_1\text{Sb}_2\text{Te}_4$  before and after crystallization. Ag atoms display significant variation in MSDs depending on the local geometry. Hopping of Ag atoms is observed for low coordinated Ag (c). In contrast, Ag with octahedral geometry does not show significant hopping. The vertical arrow in (d) represents the time of completed crystallization. In (a–c) the structures correspond to the configurations at times shown by the vertical arrows. Similar Ag MSDs were observed in  $\text{Ag}_1\text{Ge}_1\text{Sb}_2\text{Te}_4$  and are not presented here.

Ag-doped  $\text{Ge}_1\text{Sb}_2\text{Te}_4$  and present the results in Fig. 8. The MSDs of transition metals such as Zn in  $\text{Ge}_2\text{Sb}_2\text{Te}_5$  have been reported by Skelton et al. [29], where they observed large fluctuation in the MSDs even after crystallization however only a single Zn dopant was studied. Figure 8 clearly shows contrast MSDs among individual Ag atoms. We observe the local geometry of Ag atoms with the least, intermediate, and the highest diffusion as shown in Fig. 8a–c. As one might suppose, the highest diffusion is observed for the Ag with low coordination number whereas the least diffusion correspond to the Ag with octahedral geometry. As seen in Fig. 8a–c, after achieving the octahedral geometry Ag becomes less diffusive.

In the case of the Sb environment, there is almost no change in the Sb-centered bond angle distributions (up to 12% Ag) confirming that the doping of Ag does not modify the Sb environment significantly. The experimental and the theoretical analysis of the coordination numbers of Ge ( $N_{\text{Ge}}$ ) and Sb ( $N_{\text{Sb}}$ ) show that they are almost unchanged except for the sample doped with a very high Ag concentration of 42% (Fig. 4).

Both the EXAFS and PPCF analysis confirmed that Ag is mainly bonded to Te rather than Ge and Sb. From the coordination analysis (see Table 1) of Ag, we found that the

**Table 1** Ag coordination numbers obtained by integrating Ag PPCF in simulated Ag doped  $\text{Ge}_1\text{Sb}_2\text{Te}_4$  models. A cut off minimum of 3.2 Å was used.

$x$ (in %)	Ag–Ge	Ag–Sb	Ag–Te	Ag–Ag
6	–	0.6	3.6	0.4
12	0.1	0.4	3.2	0.7
42	0.3	1.0	2.4	3.0

Ag–Te bonds (ignoring Ag–Ag bonds) count for 86, 86, and 65% of the total bonds for Ag concentration of 6, 12, and 42%, respectively. Ag although prefers bonding with Te, the fraction of Ag–Te is observed to decrease as more Ag is added to the glass network due to reduced fraction of Te atoms. At the highest Ag concentration, Ag–Ag bonds start to dominate Ag–X ( $X = \text{Ge}, \text{Sb}, \text{and Te}$ ) bonds.

The coordination numbers show noticeable change for all species when the Ag concentration in  $\text{Ge}_1\text{Sb}_2\text{Te}_4$  is high (42%). These high coordination numbers for all the species cause significant modifications in the bond angle distributions as observed in Fig. 5. The appearance of a peak at  $60^\circ$  is mainly due to the species bonded with Ag. The Ge–Ag, Sb–Ag, Te–Ag, and Ag–Ag coordination numbers all increase significantly for high concentration Ag doped samples whereas Ge–Te and Sb–Te coordination number are found to decrease. The Ag coordination number of 6.7 and bond angle distribution explains the formation of Ag cluster when Ag content is very high in  $\text{Ge}_1\text{Sb}_2\text{Te}_4$ .

**4 Conclusions** In conclusion, both experimental and theoretical studies of Ag doped  $\text{Ge}_1\text{Sb}_2\text{Te}_4$  have revealed that the average Ge–Te bond length increases with Ag concentration, whereas the Sb–Te and Ag–Te bond lengths remain unchanged. The increase in the fraction of distorted octahedral Ge sites explains the net increase in Ge–Te bond lengths, and appears to be responsible for the faster crystallization of Ge–Sb–Te alloys caused by doping as confirmed by our AIMD simulations. Furthermore, the high fraction of  $N_{\text{Ag–Te}}$  as compared to  $N_{\text{Ag–Ge}}$  and  $N_{\text{Ag–Sb}}$  suggests that Ag prefers bonding with Te to Ge and Sb. Our study sheds light on the atomistic mechanism of rapid crystallization of GST alloys enhanced by Ag doping.

**Acknowledgements** The authors thank Dr. Q. Ma for assisting with the experiments. This work was supported by NSF Grant No. DMR 09-06825 and DMR 09-03225. A part of this work was performed at the DuPont–Northwestern–Dow Collaborative Access Team (DND-CAT), which is supported by E.I. DuPont de Nemours & Co., the Dow Chemical Company and Northwestern University. Use of the APS, an Office of Science User Facility operated for the U.S. Department of Energy (DOE) Office of Science by Argonne National Laboratory, was supported by the U.S. DOE under Contract No. DE-AC02-06CH11357. This work was supported by an allocation of computing time from the Ohio Supercomputer Center.

## References

- [1] M. Wuttig and N. Yamada, *Nature Mater.* **6**, 824 (2007).
- [2] S. R. Ovshinsky, in: *Non-Crystalline Materials for Optoelectronics*, edited by G. Lucovsky and M. Popescu (INOE, Bucharest, 2004), p. 1.
- [3] M. Mitkova and M. N. Kozicki, *J. Non-Cryst. Solids* **1023**, 299–302 (2002).
- [4] M. Stuchlik, P. Krecmer, and S. R. Elliott, *J. Optoelectron. Adv. Mater.* **3**(2), 361–366 (2001).
- [5] N. Yamada, E. Ohno, K. Nishiuchi, N. Akahira, K. Nagata, and M. Takao, *J. Appl. Phys.* **69**, 2849 (1991).
- [6] X. Zhou, L. Wu, Z. Song, F. Rao, M. Zhu, C. Peng, D. Yao, S. Song, B. Liu, and S. Feng, *Appl. Phys. Lett.* **101**, 142104 (2012).
- [7] Y. J. Huang, Y.-C. Chen, and T.-E. Hsieh, *J. Appl. Phys.* **106**, 034916 (2009).
- [8] G. Wang, Q. Nie, X. Shen, R. P. Wang, L. Wu, J. Fu, T. Xu, and S. Dai, *Appl. Phys. Lett.* **101**, 051906 (2012).
- [9] K. H. Song, S. W. Kim, J. H. Seo, and H. Y. Lee, *J. Appl. Phys.* **104**, 103516 (2008).
- [10] K. Wang, D. Wamwangi, S. Ziegler, C. Steimer, M. J. Kang, S. Y. Choi, and M. Wuttig, *Phys. Status Solidi A* **201**, 14 3087–3095 (2004).
- [11] K. Wang, D. Wamwangi, S. Ziegler, C. Steimer, and M. Wuttig, *J. Appl. Phys.* **96**, (10) 5557 (2004).
- [12] E. Cho, Y. Youn, and S. Han, *Appl. Phys. Lett.* **99**, 183501 (2011).
- [13] E. Cho, S. Han, D. Kim, H. Horii, and H.-S. Nam, *J. Appl. Phys.* **109**, 043705 (2011).
- [14] S. Caravati, D. Colleoni, R. Mazzarello, T. D. Kühne, M. Krack, M. Bernasconi, and M. Parrinello, *J. Phys.: Condens. Matter* **23**, 265801 (2011).
- [15] B. Prasai, G. Chen, and D. A. Drabold, *Appl. Phys. Lett.* **102**, 041907 (2013). See also X. Zhang and D. A. Drabold, *Phys. Rev. B* **62**, 15695 (2000); D. A. Drabold, *Eur. Phys. J. B* **68**, 1 (2009).
- [16] J. Hegedus and S. R. Elliott, *Nature Mater.* **7**, 399 (2008).
- [17] A. L. Ankudinov, B. Ravel, J. J. Rehr, and S. D. Conradson, *Phys. Rev. B* **58**, 7565 (1998).
- [18] B. Ravel and M. Newville, *J. Synchrotron Radiat.* **12**, 537–541 (2005).
- [19] G. Kresse and J. Furthmüller, *Phys. Rev. B* **54**(16), 11169–11186 (1996).
- [20] J. M. van Eijk, *Structural Analysis of Phase-Change Materials using X-Ray Absorption Measurements (Dissertation)*, RWTH Aachen University (2010).
- [21] A. V. Kolobov, P. Fons, A. I. Frenkel, A. L. Ankudinov, J. Tominaga, and T. Uruga, *Nature Mater.* **3**, 703 (2004).
- [22] D. A. Baker, M. A. Paesler, G. Lucovsky, and P. C. Taylor, *J. Non-Cryst. Solids* **352**, 1621–1623 (2006).
- [23] S. Caravati, M. Bernasconi, T. D. Kühne, M. Krack, and M. Parrinello, *J. Phys.: Condens. Matter* **21**, 255501 (2009).
- [24] J. Akola and R. O. Jones, *Phys. Rev. B* **76**, 235201 (2007).
- [25] B. Cai, D. A. Drabold, and S. R. Elliott, *Appl. Phys. Lett.* **97**, 191908 (2010).
- [26] J.-Y. Raty, C. Otjacques, J.-P. Gaspard, and C. Bichara, *Solid State Sci.* **12**, 193–198 (2010).
- [27] S. Caravati, M. Bernasconi, T. D. Kühne, M. Krack, and M. Parrinello, *Appl. Phys. Lett.* **91**, 171906 (2007).
- [28] J. R. Errington and P. G. Debenedetti, *Nature (London)* **409**, 318 (2001).
- [29] J. M. Skelton, T. H. Lee, and S. R. Elliott, *Appl. Phys. Lett.* **101**, 024106 (2012).